

A New Theobromine-Based EGFRWT and EGFR T790M Inhibitor and Apoptosis Inducer: Design, Semi-Synthesis, Docking, DFT, MD Simulations, and In Vitro Studies

Authors:

Eslam B. Elkaeed, Reda G. Yousef, Hazem Elkady, Aisha A. Alsouk, Dalal Z. Husein, Ibrahim M. Ibrahim, Mohamed Alswah, Heba S. A. Elzahabi, Ahmed M. Metwaly, Ibrahim H. Eissa

Date Submitted: 2023-02-21

Keywords: anti-proliferative, theobromine, EGFR inhibitors, MD simulation, docking

Abstract:

The essential pharmacophoric structural properties were applied to design a new derivative of theobromine as an antiangiogenic EGFR inhibitor. The designed candidate is a (para-nitrophenyl)acetamide derivative of the natural alkaloid, theobromine (T-2-PNPA). The potentialities of T-2-PNPA to inhibit the EGFR protein were studied computationally in an extensive way. Firstly, the molecular docking against EGFRWT and EGFR T790M demonstrated T-2-PNPA's capabilities of binding with the targeted receptors. Then, the MD experiments (for 100 ns) illustrated through six different studies the changes that occurred in the energy as well as in the structure of EGFR?T-2-PNPA complex. Additionally, an MM-GBSA analysis determined the exact energy of binding and the essential residues. Furthermore, DFT calculations investigated the stability, reactivity, and electrostatic potential of T-2-PNPA. Finally, ADMET and toxicity studies confirmed both the safety as well as the general likeness of T-2-PNPA. Consequently, T-2-PNPA was prepared for the in vitro biological studies. T-2-PNPA inhibited EGFRWT and EGFR T790M with IC50 values of 7.05 and 126.20 nM, respectively, which is comparable with erlotinib activities (5.91 and 202.40, respectively). Interestingly, T-2-PNPA expressed cytotoxic potentialities against A549 and HCT-116 cells with IC50 values of 11.09 and 21.01 μ M, respectively, which is again comparable with erlotinib activities (6.73 and 16.35, respectively). T-2-PNPA was much safer against WI-38 (IC50 = 48.06 μ M) than erlotinib (IC50 = 31.17 μ M). The calculated selectivity indices of T-2-PNPA against A549 and HCT-116 cells were 4.3 and 2.3, respectively. This manuscript presents a new lead anticancer compound (T-2-PNPA) that has been synthesized for the first time and exhibited promising in silico and in vitro anticancer potentialities.

Record Type: Published Article

Submitted To: LAPSE (Living Archive for Process Systems Engineering)

Citation (overall record, always the latest version):

LAPSE:2023.0820

Citation (this specific file, latest version):

LAPSE:2023.0820-1

Citation (this specific file, this version):








LAPSE:2023.0820-1v1

DOI of Published Version: <https://doi.org/10.3390/pr10112290>

License: Creative Commons Attribution 4.0 International (CC BY 4.0)

Article

A New Theobromine-Based EGFR^{WT} and EGFR^{T790M} Inhibitor and Apoptosis Inducer: Design, Semi-Synthesis, Docking, DFT, MD Simulations, and In Vitro Studies

Eslem B. Elkaeed ¹, Reda G. Yousef ², Hazem Elkady ², Aisha A. Alsouk ³, Dalal Z. Husein ⁴, Ibrahim M. Ibrahim ⁵, Mohamed Alswah ⁶, Heba S. A. Elzahabi ⁷, Ahmed M. Metwaly ^{8,9,*} and Ibrahim H. Eissa ^{2,*}

- ¹ Department of Pharmaceutical Sciences, College of Pharmacy, Almaarefa University, Riyadh 13713, Saudi Arabia
- ² Pharmaceutical Medicinal Chemistry & Drug Design Department, Faculty of Pharmacy (Boys), Al-Azhar University, Cairo 11884, Egypt
- ³ Department of Pharmaceutical Sciences, College of Pharmacy, Princess Nourah bint Abdulrahman University, Riyadh 11671, Saudi Arabia
- ⁴ Chemistry Department, Faculty of Science, New Valley University, El-Kharja 72511, Egypt
- ⁵ Biophysics Department, Faculty of Science, Cairo University, Cairo 12613, Egypt
- ⁶ Pharmaceutical Organic Chemistry Department, Faculty of Pharmacy (Boys), Al-Azhar University, Nasr City 11884, Egypt
- ⁷ Pharmaceutical Medicinal Chemistry & Drug Design Department, Faculty of Pharmacy (Girls), Al-Azhar University, Cairo 11884, Egypt
- ⁸ Pharmacognosy and Medicinal Plants Department, Faculty of Pharmacy (Boys), Al-Azhar University, Cairo 11884, Egypt
- ⁹ Biopharmaceutical Products Research Department, Genetic Engineering and Biotechnology Research Institute, City of Scientific Research and Technological Applications (SRTA-City), Alexandria 21934, Egypt
- * Correspondence: ametwaly@azhar.edu.eg (A.M.M.); ibrahimeissa@azhar.edu.eg (I.H.E.)



Citation: Elkaeed, E.B.; Yousef, R.G.; Elkady, H.; Alsouk, A.A.; Husein, D.Z.; Ibrahim, I.M.; Alswah, M.; Elzahabi, H.S.A.; Metwaly, A.M.; Eissa, I.H. A New Theobromine-Based EGFR^{WT} and EGFR^{T790M} Inhibitor and Apoptosis Inducer: Design, Semi-Synthesis, Docking, DFT, MD Simulations, and In Vitro Studies. *Processes* **2022**, *10*, 2290. <https://doi.org/10.3390/pr10112290>

Academic Editors: Fabio Carniato, Nicolas Lepareur and Nicolas Noiret

Received: 11 August 2022

Accepted: 27 October 2022

Published: 4 November 2022

Publisher's Note: MDPI stays neutral with regard to jurisdictional claims in published maps and institutional affiliations.



Copyright: © 2022 by the authors. Licensee MDPI, Basel, Switzerland. This article is an open access article distributed under the terms and conditions of the Creative Commons Attribution (CC BY) license (<https://creativecommons.org/licenses/by/4.0/>).

Abstract: The essential pharmacophoric structural properties were applied to design a new derivative of theobromine as an antiangiogenic EGFR inhibitor. The designed candidate is a (paranitrophenyl)acetamide derivative of the natural alkaloid, theobromine (**T-2-PNPA**). The potentialities of **T-2-PNPA** to inhibit the EGFR protein were studied computationally in an extensive way. Firstly, the molecular docking against EGFR^{WT} and EGFR^{T790M} demonstrated **T-2-PNPA**'s capabilities of binding with the targeted receptors. Then, the MD experiments (for 100 ns) illustrated through six different studies the changes that occurred in the energy as well as in the structure of EGFR–**T-2-PNPA** complex. Additionally, an MM-GBSA analysis determined the exact energy of binding and the essential residues. Furthermore, DFT calculations investigated the stability, reactivity, and electrostatic potential of **T-2-PNPA**. Finally, ADMET and toxicity studies confirmed both the safety as well as the general likeness of **T-2-PNPA**. Consequently, **T-2-PNPA** was prepared for the in vitro biological studies. **T-2-PNPA** inhibited EGFR^{WT} and EGFR^{T790M} with IC₅₀ values of 7.05 and 126.20 nM, respectively, which is comparable with erlotinib activities (5.91 and 202.40, respectively). Interestingly, **T-2-PNPA** expressed cytotoxic potentialities against A549 and HCT-116 cells with IC₅₀ values of 11.09 and 21.01 μM, respectively, which is again comparable with erlotinib activities (6.73 and 16.35, respectively). **T-2-PNPA** was much safer against WI-38 (IC₅₀ = 48.06 μM) than erlotinib (IC₅₀ = 31.17 μM). The calculated selectivity indices of **T-2-PNPA** against A549 and HCT-116 cells were 4.3 and 2.3, respectively. This manuscript presents a new lead anticancer compound (**T-2-PNPA**) that has been synthesized for the first time and exhibited promising in silico and in vitro anticancer potentialities.

Keywords: anti-proliferative; theobromine; EGFR inhibitors; MD simulation; docking

1. Introduction

According to estimates of the WHO, cancer will be the second leading cause of death in the next few years [1]. Cancer therapy is a big challenge for medicinal chemists who aim to develop drugs that inhibit cancer growth by interacting with specific molecular targets and causing damage to the cancer cells [2]. There are various studies linking tumor growth and survival to the increased vascularity (angiogenesis) in cancer cells [3]. Thus, a potential strategy to combat cancer is to counteract this phenomenon [4]. Cancer cells grow and undergo angiogenesis through epidermal growth factor receptors (EGFRs) [5]. A cascade of downstream signaling pathways is triggered by EGFR's overexpression of, which stimulates proliferation and differentiation, as well as survival of cells [6]. The link between the promotion of solid tumor growth and the elevated levels of EGFR was discovered in multiple types of cancer [7]. Additionally, a reduction in survival rate has been associated with increased EGFR expression in several types of cancer, and EGFR expression in these cancers has served as a strong prognostic indicator [8]. Fortunately, researchers were able to target cancer cells with EGFR receptors due to their overexpression in cancer cells as compared to normal cells [9].

Natural products were historically the most essential base of drug development [10,11]. Presently, as many as one-third of the new FDA-approved drugs in the last two decades are derived from natural sources [12]. In the field of natural anticancer drug discovery, xanthine derivatives showed a variety of antimutagenic activities against ovarian [13], prostate [14], leukemia [15], and breast [15] cancers. Theobromine is a xanthine alkaloid that was first discovered in 1841 [16]. In addition to being found in chocolate, it is an ingredient of other foods such as leaves from the tea plant [17]. Through in vitro and in vivo testing, theobromine showed promising anticancer activities by inhibiting DNA synthesis and inhibiting the growth of glioblastoma multiforme (U87MG cell line) [18]. Similarly, theobromine inhibited the angiogenesis in lung cancer [19]. It also exhibited promising antiangiogenic activity via inhibition of VEGF in both in vivo and in vitro testing of ovarian cancer [20].

The study of the structure–activity relationship leads to the discovery and repurposing of more potent drugs and enhances drug-likeness, pharmacokinetics, and pharmacodynamics of new drugs [21]. Computational chemistry is used for researching chemistry problems using software employing many techniques. Computational chemistry was widely used in the pharmaceutical industry for studying how potential drugs interact with biomolecules [22]. The computational chemistry applications starts from the molecular and drug design [23] and extends to the structure-based approaches as docking and MD simulations [24] as well as the ligand-based approaches such ADMET [25,26], DFT [27], structure similarity [28], and pharmacophore assessment [29].

There are three generations of the FDA-approved anticancer drugs targeting EGFR. The first generation (such as erlotinib I [30]) was very active against the non-small-cell lung cancer. The second generation (such as afatinib II [31]) overcame EGFR resistance due to mutation. The third generation (such as olmutinib III [32] and avitinib IV [33]) overcome the second generation's induced toxicity and showed improved activities towards EGFR^{T790M} over the EGFR^{WT}.

In the literature, some 1*H*-pyrazolo[3,4-*d*]pyrimidine derivatives such as compounds V [34] and VI [35] were reported to have good EGFR inhibitory activity. Moreover, our team discovered some 1*H*-pyrazolo[3,4-*d*]pyrimidine derivatives (such as compound VII [36]) and thieno[2,3-*d*]pyrimidine derivatives (such as compound VIII [37]). These compounds were proved to have promising EGFR kinase inhibitory activity with good cytotoxic activity.

We present in this manuscript the design, in silico and in vitro examinations of a new derivative of theobromine. The chemical compound (2-(3,7-Dimethyl-2,6-dioxo-2,3,6,7-tetrahydro-1*H*-purin-1-yl)-*N*-(4-nitrophenyl)acetamide, **T-2-PNPA**) was synthesized and introduced for the first time by our team. Then, **T-2-PNPA** showed promising in silico and in vitro anticancer potentialities.

Rationale

As shown in Figure 1, four essential features should be present in the chemical structure of EGFR inhibitors in order to bond correctly with the active site [38]. These features are a flat hetero aromatic system, an NH spacer, a terminal hydrophobic head, and a hydrophobic tail. These moieties have the potentialities to occupy the adenine-binding pocket, the linker region, the hydrophobic region I, and the hydrophobic region II, respectively of the EGFR active site [39–41].

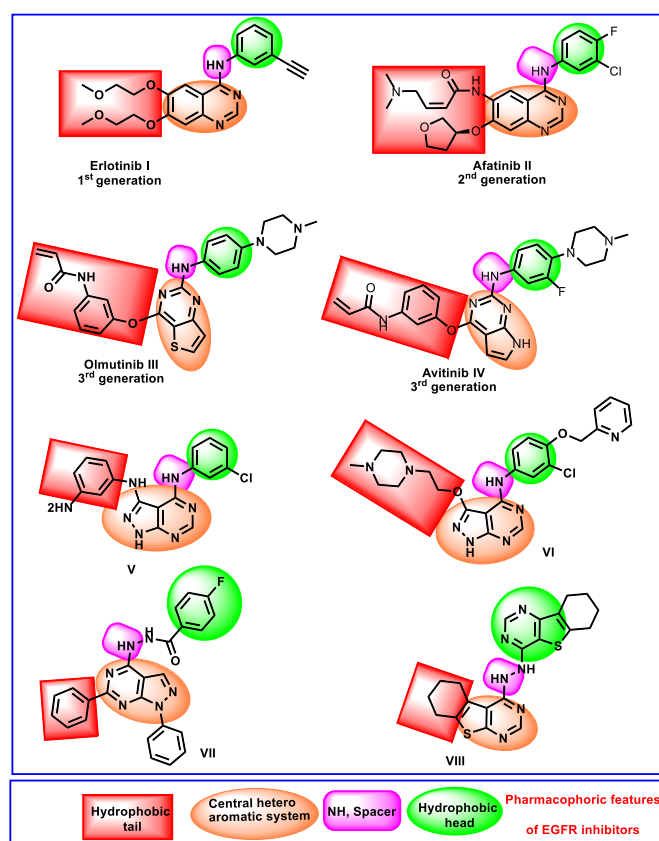


Figure 1. Some reported EGFR inhibitors show the essential pharmacophoric features.

Observing the structures of Olmutinib III, avitinib IV, compounds V, VI, VII, and VIII, there are diverse hetero aromatic systems such as thieno[3,2-*d*]pyrimidine, 7*H*-pyrrolo[2,3-*d*]pyrimidine, and 1*H*-pyrazolo[3,4-*d*]pyrimidine. These hetero aromatic systems can occupy the adenine-binding pocket of the EGFR active site. Interestingly, all these aromatic systems are composed of pyrimidine moiety fused with a five-membered ring. Depending on the ligand-based drug design approach, we designed a theobromine derivative that kept the main features of the lead compounds (III–VIII).

As shown in Figure 2, we have designed a new compound (2-(3,7-Dimethyl-2,6-dioxo-2,3,6,7-tetrahydro-1*H*-purin-1-yl)-*N*-(4-nitrophenyl)acetamide, **T-2-PNPA**) that has a theobromine moiety as a hetero aromatic system to occupy the adenine-binding pocket. The theobromine moiety is composed of a pyrimidine moiety fused with the five-membered 1*H*-imidazole ring, meaning that it is considered a good ring equivalent of the thieno[3,2-*d*]pyrimidine, 7*H*-pyrrolo[2,3-*d*]pyrimidine, and 1*H*-pyrazolo[3,4-*d*]pyrimidine moieties. Additionally, the acetamide moiety was designed as a linker which may increase the flexibility of the designed compound and consequently increase its affinity against the target protein. The *p*-nitrobenzene moiety was designed with a hydrophobic head to occupy the hydrophobic region I. Furthermore, the methyl group at the 7-position of theobromine moiety was utilized as a hydrophobic tail to occupy the hydrophobic region II (Figure 2).

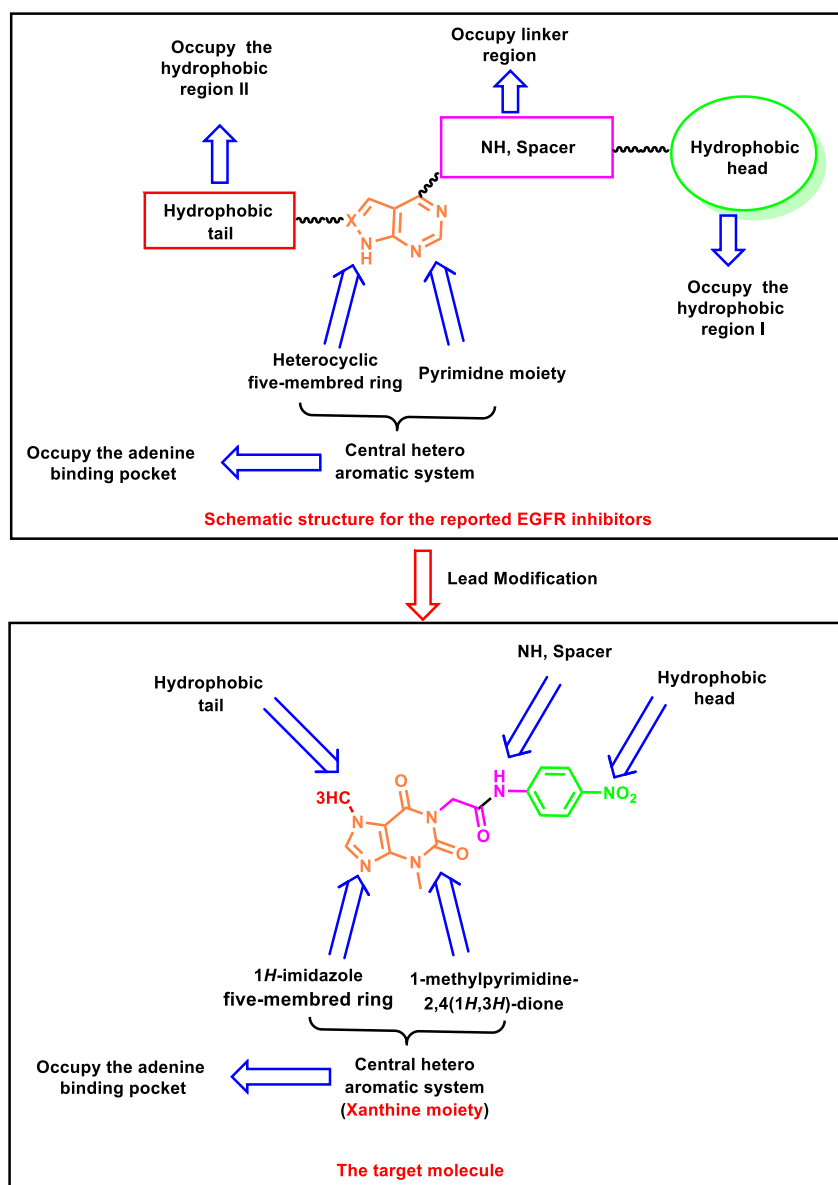


Figure 2. The rationale for the molecular design of **T-2-PNPA** as a potential EGFR inhibitor.

2. Results and Discussion

2.1. Molecular Docking

2.1.1. Molecular Docking Studies against the Wild EGFR Protein (EGFR^{WT})

We decided to proceed with a molecular docking study of **T-2-PNPA** against the ATP-binding site of wild EGFR (EGFR^{WT}; PDB: 4HJO) using erlotinib as a standard. The validation step generates an acceptable RMSD value of 1.40 (Supplementary Materials). Furthermore, the binding mode of erlotinib has shown the essential hydrogen bond (HB) interaction with the key amino acid residue, Met 769, and this was consistent with the one described in the literature [42] as presented in Figure 3.

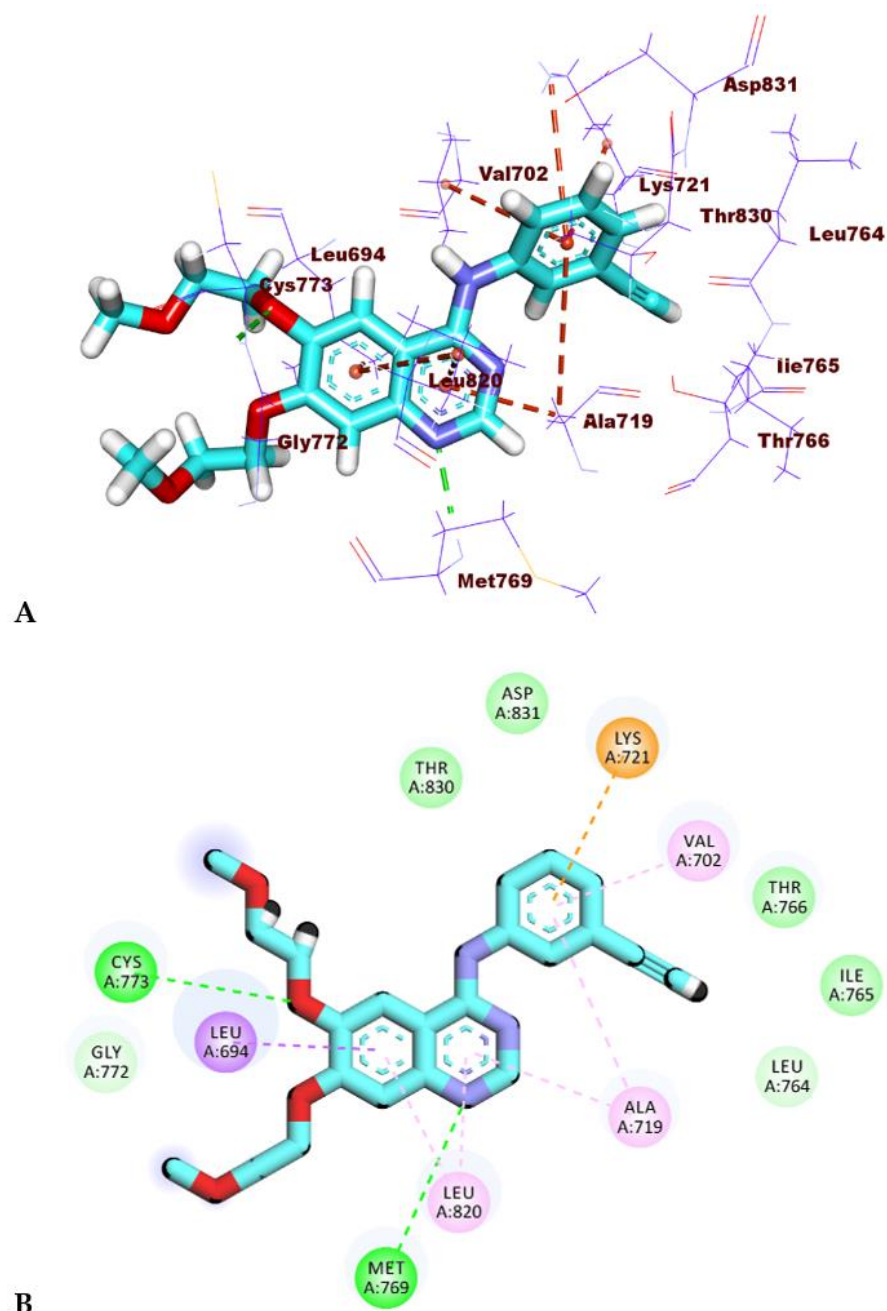


Figure 3. (A) 3D and (B) 2D interaction pattern of erlotinib in of EGFR^{WT} active site.

Similar to how erlotinib binds, T-2-PNPA was able to employ its 6-oxo group of the 1*H*-purine moiety to anchor the adenine pocket via a key HBing formation with Met793. Additionally, in the same pocket, the whole nucleus (3,7-dimethyl-2,6-dioxo-2,3,6,7-tetrahydro-1*H*-purine moiety) was involved in three hydrophobic bond (HI)s with Leu694 and Cys773. Regarding the hydrophobic pocket, the 4-nitrophenyl moiety was engaged in two pi–pi and two electrostatic interactions with Ala719, Val702, Lys721, and Asp831, respectively. As previously stated, our assumption was that the nitro group would interact with the molecular target via a charge-reinforced HB or electrostatic charge (Figure 4).

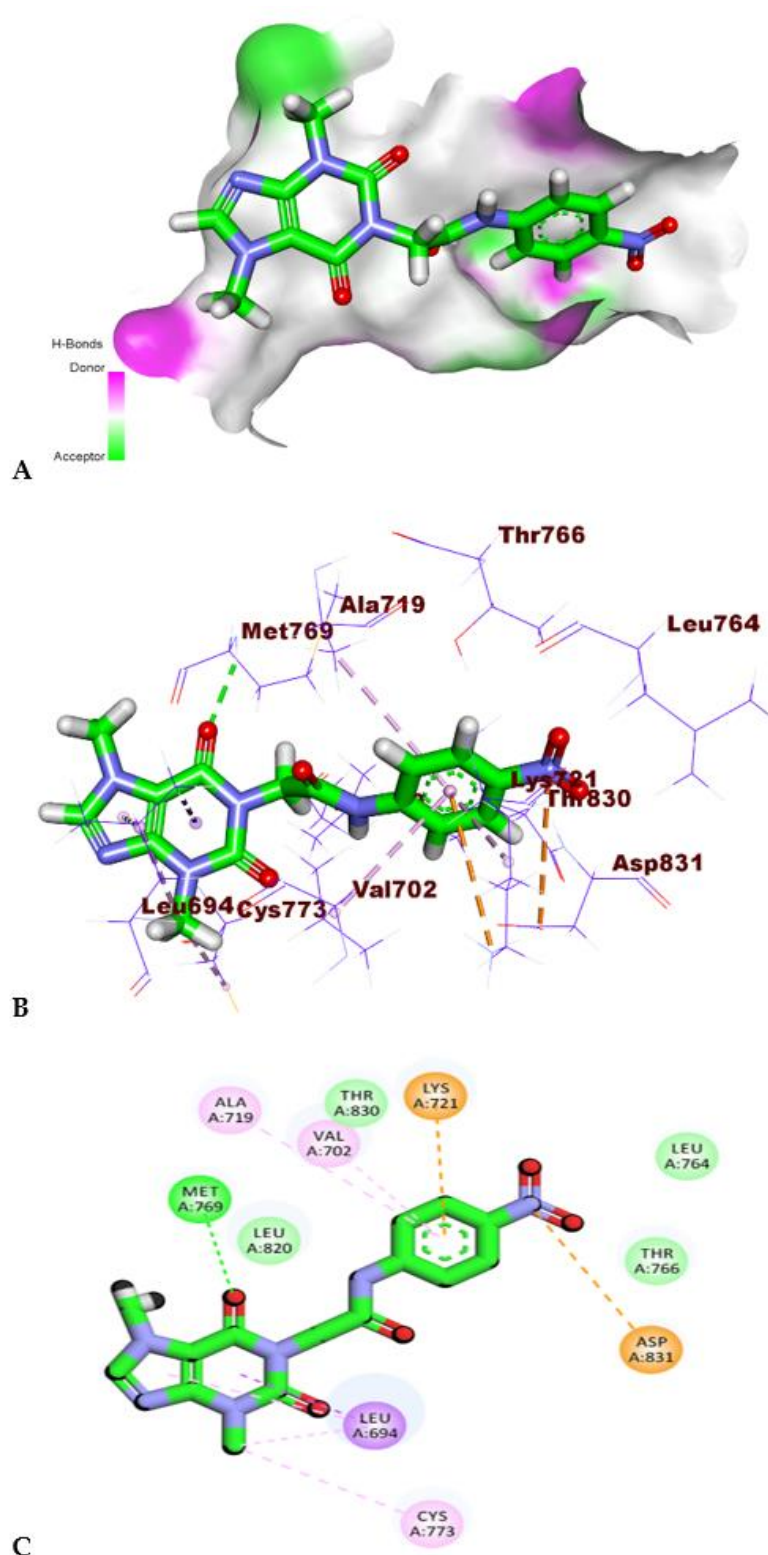


Figure 4. (A) Mapping surface (MS), (B) 3D, and (C) 2D interaction pattern of T-2-PNPA with EGFR^{WT} active site.

2.1.2. Molecular Docking Studies against Mutant EGFR Protein (EGFR^{T790M})

To reinforce the above findings, the docking results of T-2-PNPA against the mutant type of EGFR (EGFR^{T790M}, PDB: 3W2O) were discussed. Initially, aligning the co-crystallized ligand (TAK-285) in the mutant EGFR^{T790M} generated an RMSD value of 1.11. This value validated the docking procedure (Supplementary Materials). The binding profile of TAK-

285 to the EGFR^{T790M} active site is shown in Figure 5. The obtained results and the reported data harmonized completely.

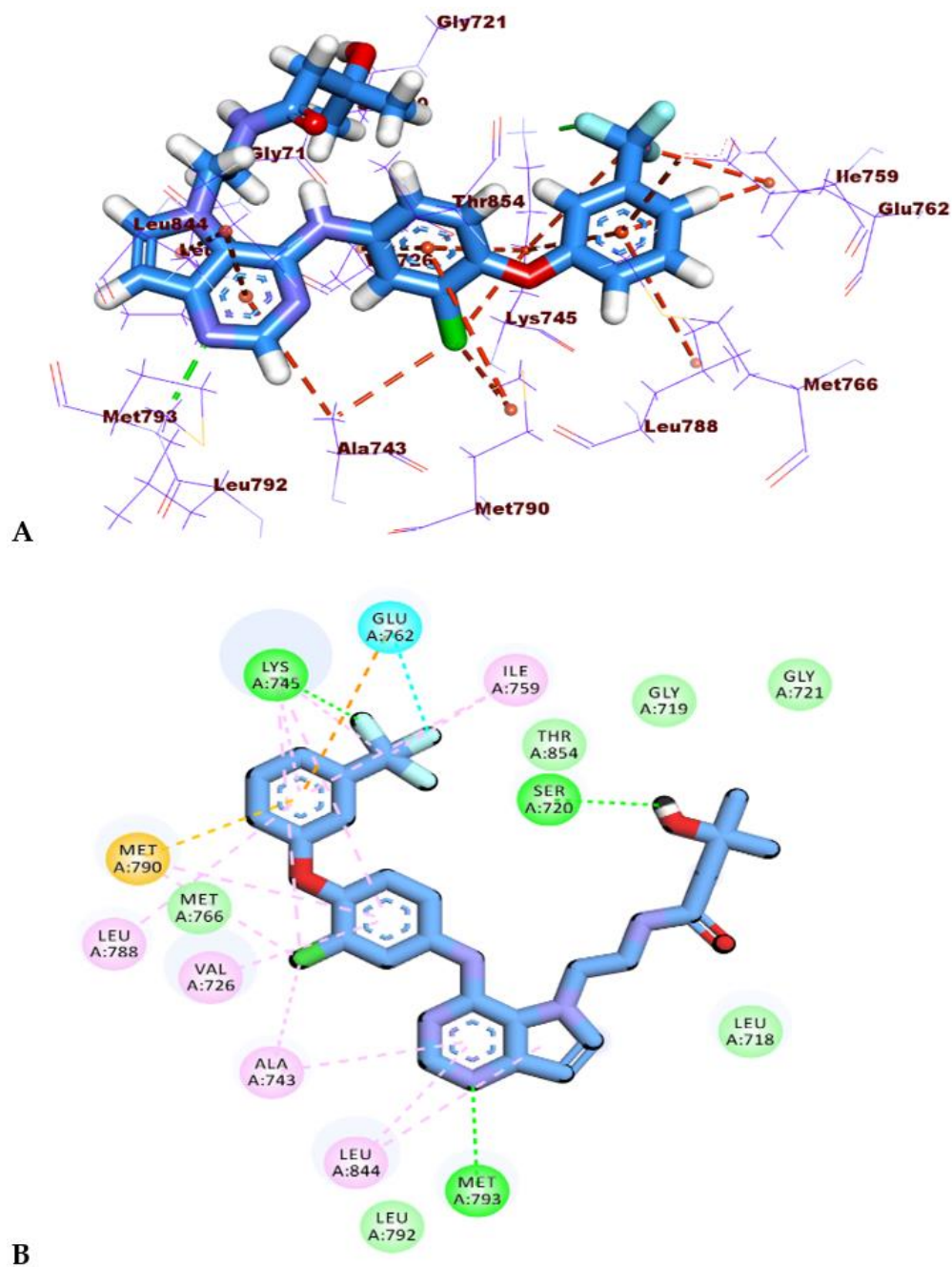


Figure 5. (A) 3D and (B) 2D interaction pattern of TAK-285 in EGFR^{T790M} active site.

The designed compound, T-2-PNPA, was stacked onto the EGFR^{T790M} catalytic site similarly to the native ligand, as shown in Figure 6. In the adenine pocket, the 3,7-dimethyl-2,6-dioxo-2,3,6,7-tetrahydro-1*H*-purine moiety achieved eight HIs with Leu844, Leu718, Ala743, and Met793 as well as two HBs with Thr845 and Met793. Moreover, two electrostatic interactions were observed in the hydrophobic pocket via the interaction of *p*-nitrophenyl moiety with Lys745 and Glu762.

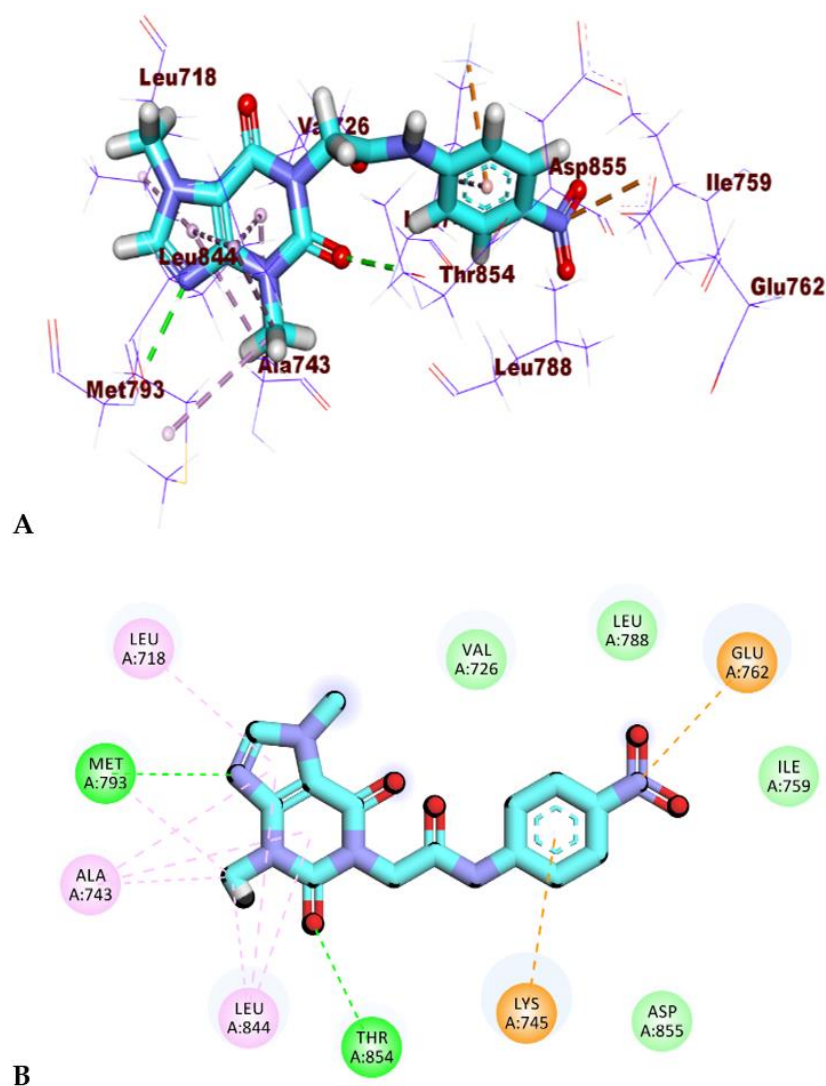


Figure 6. (A) 3D and (B) 2D interaction pattern of T-2-PNPA with the EGFR^{T790M} active site.

2.2. MD Simulations

The MD analyses performed on the production run of 100 ns show that, overall, the system is stable. The RMSD plot (Figure 7A) shows equilibrated values for EGFR and EGFR–T-2-PNPA complex (blue and green curve, respectively) through the whole trajectory with an average value of 2.9 Å. Interestingly, the RMSD of the T-2-PNPA (red curve) shows very large fluctuations during the trajectory which indicates its large free motion inside the binding pocket, however, its distance from the center of mass of EGFR remains nearly constant with an average of 11.62 Å (Figure 7F). The RoG (Figure 7B), and SASA (Figure 7C) show a stable protein fluctuation with an average of 19.79 Å, 15755 Å², respectively. H-bonds formed between the T-2-PNPA and EGFR (Figure 7D) shows that at least one H-bond is formed in 214 frames out of 1000 frames (21.4%). The amino acids' fluctuation was depicted in the RMSF plot (Figure 7E) showing low fluctuation value (less than 2 Å) except for the G695:G700 (reaching 3.6 Å), and E842:V852 loop regions (reaching 3.6 Å) and the free C-terminal (reaching 7 Å).

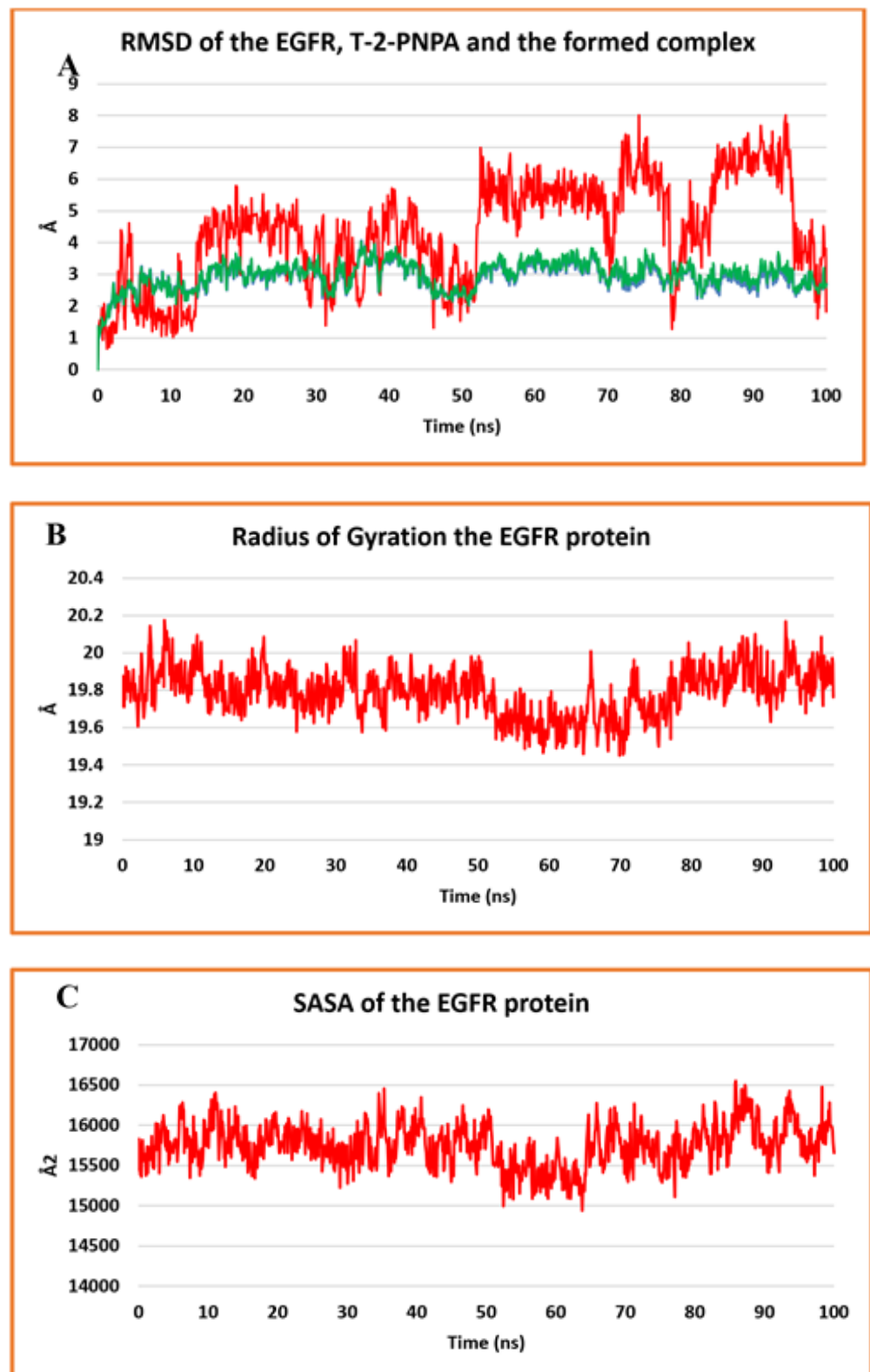


Figure 7. Cont.

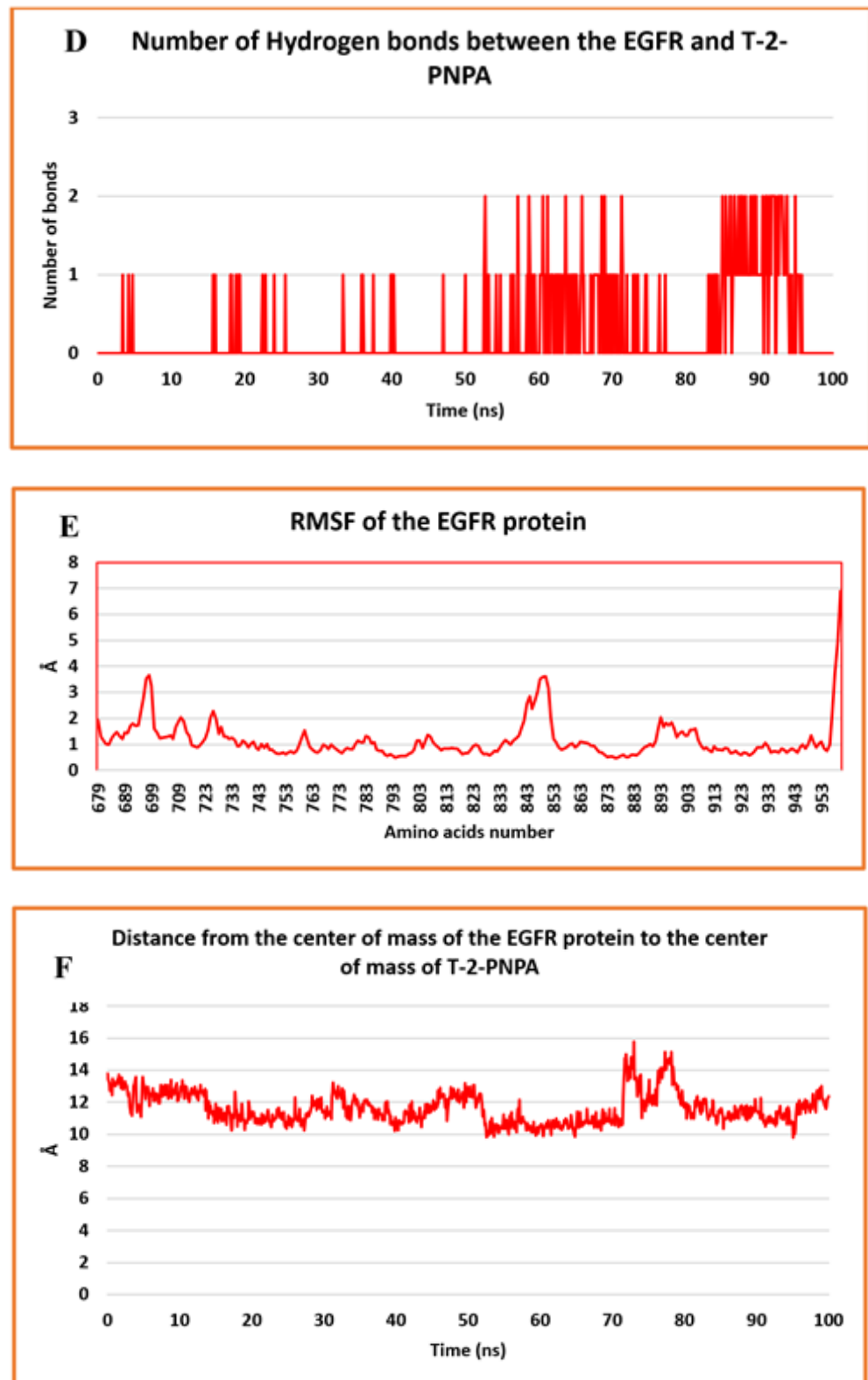


Figure 7. MD simulation's findings computed from the trajectory. (A) RMSD: EGFR (blue), T-2-PNPA (red), and EGFR–T-2-PNPA complex (green), (B) RoG (C) SASA (D) HBs' number changes (E) RMSF, and (F) Center of Mass distance between the T-2-PNPA and EGFR.

2.3. MM-GBSA

The analysis of the obtained binding free energy employing MM-GBSA (Figure 8) shows the contribution of every component to the energy of binding. The EGFR–T-2-PNPA

complex expressed a binding's average energy of -22.35 kcal/mol. The most favorable contributors are the Van Der Waals interactions followed by the electrostatic interaction with average energy values of -36.92 and -19.38 kcal/mol, respectively. Additionally, we performed a decomposition study (Figure 9) to identify the amino acids that contribute within 1 nm of the EGFR-T-2-PNPA complex, which have the most significant contribution to the binding. L694, V702, K721, and L820 are the amino acid residues that have contributed with an energy value less than -1 kcal/mol (-2.69 , -1.97 , -1.22 , and -1.13 kcal/mol, respectively). On the other hand, D776 ($+0.46$ kcal/mol), and D831 ($+0.7$ kcal/mol) show a positive free energy (non-favorable) contribution to the binding to the EGFR protein.

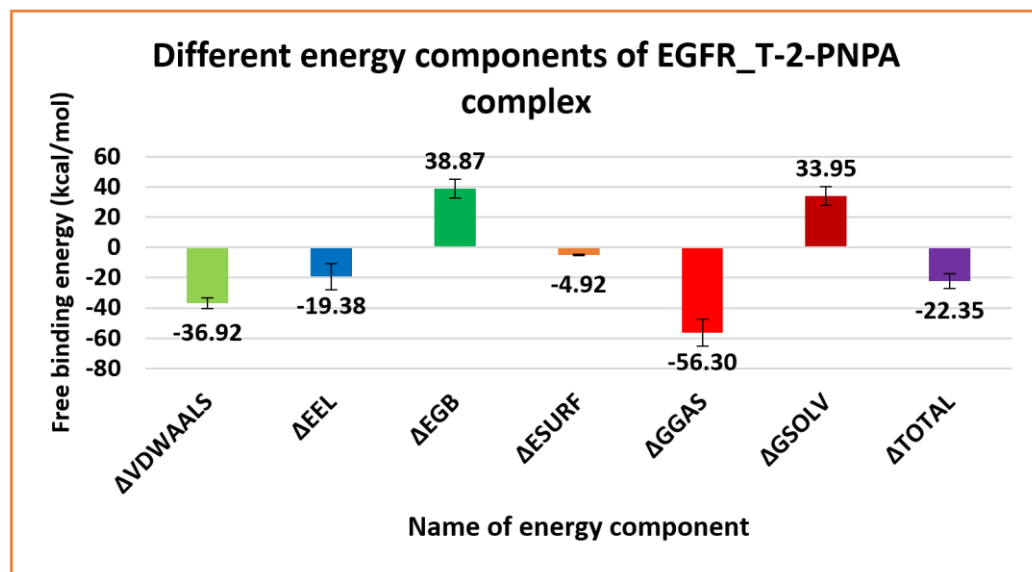


Figure 8. MM-GBSA of EGFR-T-2-PNPA complex showing energetic components and their average energy values. Bars denote the standard deviation.

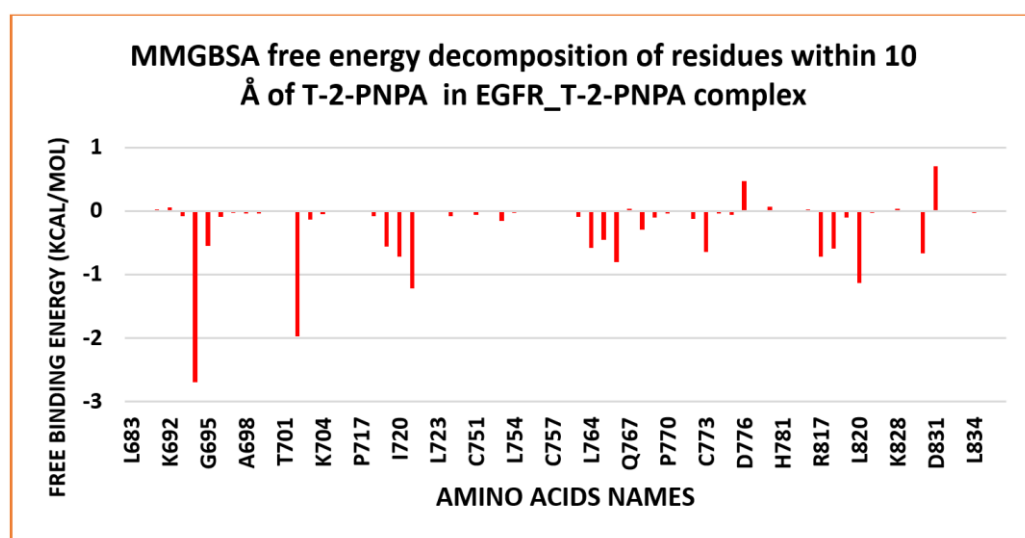


Figure 9. Binding free energy decomposition of the EGFR-T-2-PNPA complex.

2.4. PLIP Study

As already known, MD simulation can produce a very large number of frames that can have a minimal difference. Many methods to reduce the number of frames by selecting the ones that are conformationally different have been developed such as clustering and wavelet analysis [43]. In this work, we have utilized the clustering technique to reduce

the data dimensionality and to obtain a representative frame for every produced cluster. As clarified in the experimental section (Supplementary Materials), cluster numbers were automatically calculated by the elbow method to produce four successive clusters. For each one, the PLIP webserver was employed to identify both number and types of interactions between T-2-PNPA and EGFR (Table 1). As can be seen, HIs are the common type of interactions between T-2-PNPA and EGFR with a total of 11 HIs compared to only three H-bonds. Additionally, a .pse file was generated to understand the 3D conformation of the T-2-PNPA interactions inside EGFR (Figure 10).

Table 1. The detected interactions from the PLIP webserver.

Cluster Number	Number of HIs	Amino Acids in Receptor	Number of HBs	Amino Acids in Receptor
C1	2	L694-L820	0	None
C2	3	A719-K721-T766	0	None
C3	3	V702-K721-T830	1	S696
C4	3	V702 (2)-T830	2	R817-N818

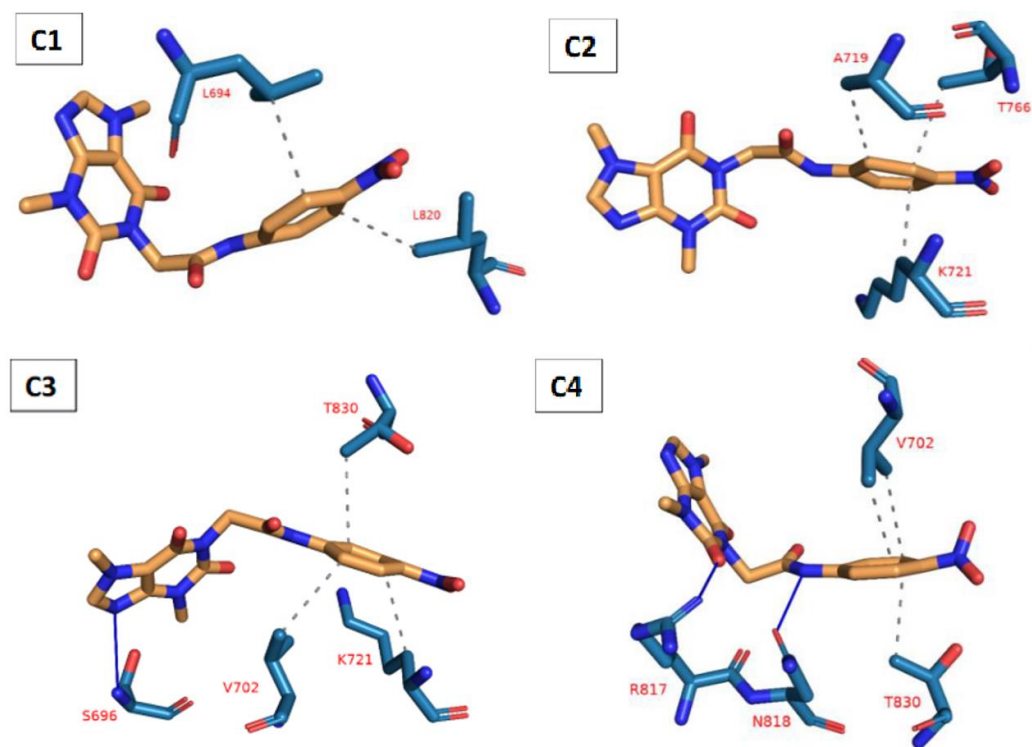


Figure 10. Interactions obtained from the PLIP of every cluster. HB: blue solid line, HI: dashed gray line, amino acids: blue sticks representation, and T-2-PNPA: orange sticks representation.

2.5. DFT Studies

Density functional theory (DFT) is one of the best computational techniques for quantitatively predicting and rationalizing the reactivity of biomolecules. The predicted properties of reasonable accuracy can be obtained by DFT. Many quantum chemical parameters, such as the lowest unoccupied molecular orbital energy, ELUMO, and the highest occupied molecular orbitals energy, EHOMO, gap's energy (ΔE) EHOMO–ELUMO, global electrophilicity (ω), dipole moment (D), electronegativity (χ), softness (σ), and chemical hardness (η), all affect how surface atoms interact electronically with the target.

2.5.1. Geometry Optimization

The level of theory used for all calculations was DFT/B3LYP/6-311G++(d,p). Without any restrictions, T-2-PNPA optimization was carried out and depicted in Figure 11. The intermediate and reactant were bound via the C14–N2 bond. The C14–N2 bond length and the two angles on both sides were recorded on the optimized structure, Figure 11. The dipole moment (Dm), which indicates the interaction within the compound, also determines the molecule's polarity. According to Table 2, the Dm value is 11.321 Debye and the measured ground total energy (TE) is $-34,966.4$ eV.

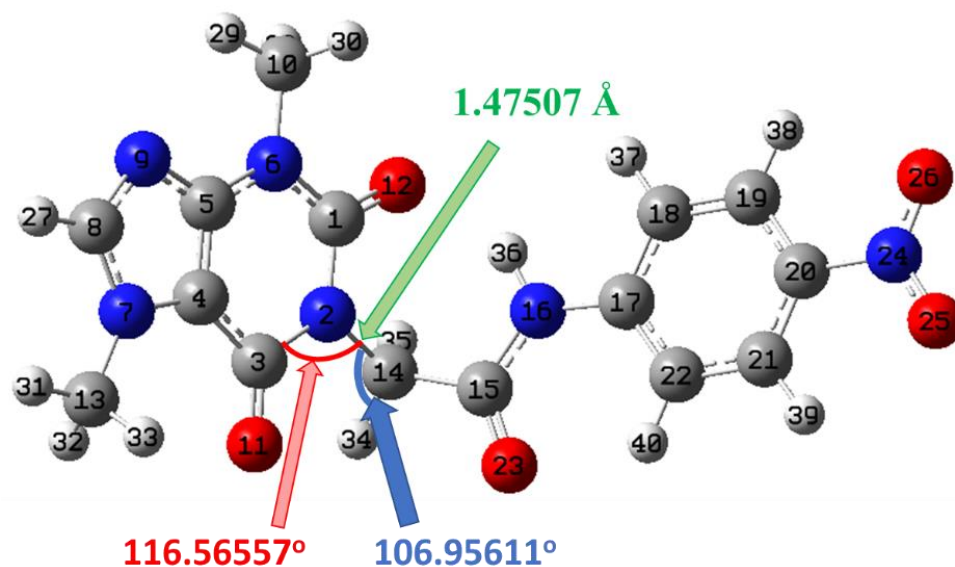


Figure 11. The optimized chemical structure of T-2-PNPA at B3LYB/6-311G++(d,p) basis set.

Table 2. The calculated global reactivity indices and energetic parameters for T-2-PNPA.

IP	EA	μ (eV)	χ (eV)	η (eV)	σ (eV)	ω (eV)	Dm (Debye)	TE (eV)	ΔN_{max}	ΔE (eV)
-2.616	-6.876	-4.746	4.746	-2.130	-0.469	-23.989	11.321	-34966.4	-2.228	23.989

2.5.2. Frontier Molecular Orbital Analysis (FMO) Analysis

All chemical reactions greatly benefit from orbital analysis. In reality, molecular orbitals (MOs) are crucial for a deeper comprehension of chemical processes and electrical electronic characteristics. Around the year 1952, Fukui proposed the border orbital theory, which connects reactivity to the characteristics of the HOMO and LUMO molecular orbitals.

The computed energy gap (E_{gap}) between T-2-PNPA's HOMO and LUMO is -4.260 eV according to the FMO study, and the sketch diagram is shown in Figure 12. The calculated E_{gap} value is low which indicates a small HOMO–LUMO gap in the border orbitals. The molecule under investigation, T-2-PNPA, showed high polarizability and chemical reactivity according to the calculated Dm and E_{gap} values [44]. Table 2 shows the computed energies for HOMO (E_{HOMO}), LUMO (E_{LUMO}), and E_{gap} .

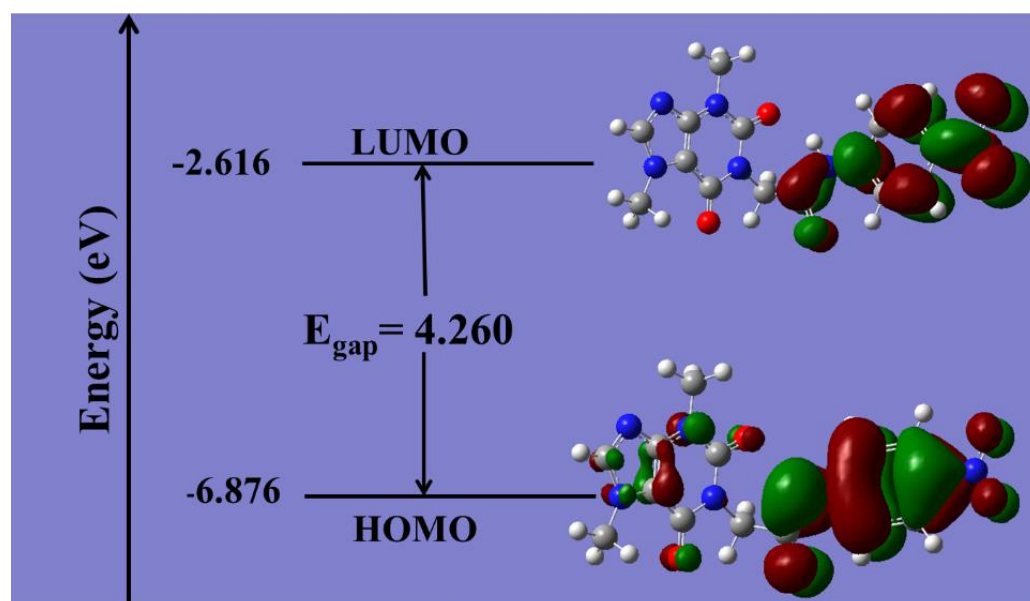


Figure 12. The FMO analysis; HOMO and LUMO of T-2-PNPA at the ground state at B3LYB/6-311++G(d,p).

2.5.3. Global Reactive Indices and Total Density of State (TDOS)

The global reactivity indices provides information about the reactivity or inhibitory ability of a compound from chemical point of view. It can be efficiently obtained via quantum calculations [45]. Theoretical static calculations are used to derive the reactivity indices involving molecular orbitals [46]. Global reactivity indices that characterize a molecule's capability to be stable or reactive include global chemical hardness (η) and softness (σ). When a molecule's softness value (σ) is high and its hardness value (η) is low, it is found to be a strong inhibitor. The ionization potential (IP), energy change (ΔE), maximal charge acceptance (N_{\max}), electrophilicity (ω), chemical potential (μ), electronegativity (χ), global chemical softness (σ), global chemical hardness (η), and electron affinity (EA) of the molecule were all calculated using Koopmans' theory:

$$IP = -E_{\text{HOMO}}$$

$$EA = -E_{\text{LUMO}}$$

$$\mu = (IP + EA)/2$$

$$\eta = (IP - EA)$$

$$\chi = -\eta$$

$$\omega = \mu^2/(2\eta)$$

$$\sigma = 1/\eta$$

$$\Delta N_{\max} = -(\mu/\eta)$$

$$\Delta E = -\omega$$

$$E_{\text{gap}} = E_{\text{LUMO}} - E_{\text{HOMO}}$$

Due to the possibility of quasi-degenerate levels in the border region, LUMO and HOMO could not give an accurate description of FMO. Although FMO analysis is important, the HOMO–LUMO theory has some limitations and new efforts are necessary to understand when and how the HOMO energy works and does not work [47]. The occupied states' number per unit volume is determined at equilibrium by a chemical system's probability distribution function and the density of its states. This quantity is used to investigate

the physical characteristics of chemical systems. Figure 13 shows that T-2-PNPA has a considerable narrow energy gap, as determined by the TDOS analysis, and the orbitals under the HOMO orbital had the highest reported intensities. Such findings highlighted the potency of the prospective inhibitor.

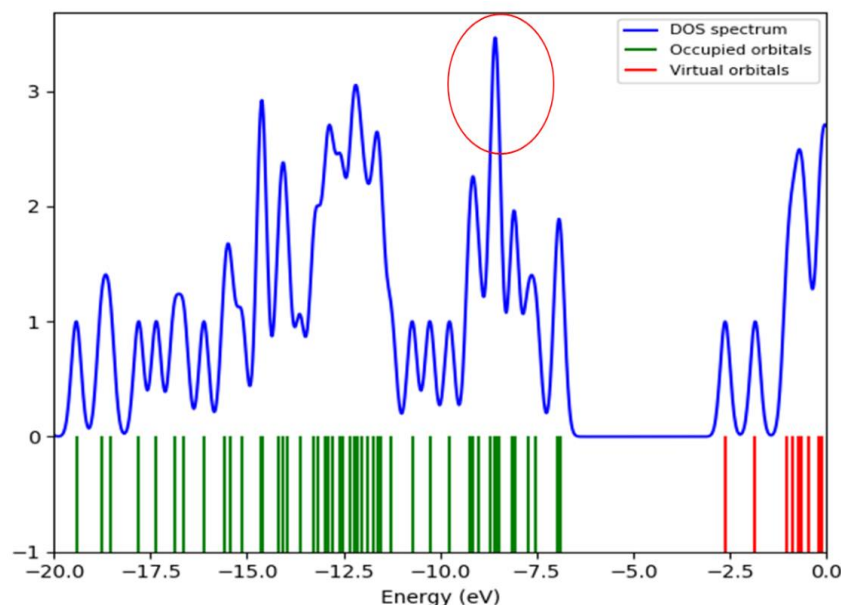


Figure 13. Molecular frontier orbital spectrum, their energies and TDOS were calculated at B3LYP/6-311++G(d,p).

2.5.4. TED and ESP Surface Potential Maps

The total electron density surface (TED), also known as the potential (electron + nuclei) mapping, shows the distribution, size, shape, and dipole moments of the compound's ESP. Figure 14 illustrates the TED and ESP of T-2-PNPA graphically. Green, blue, yellow and red sections indicate, respectively, the neutral electron, electron deficient, slightly rich, and electron-rich zones. The most negative potential zones are found around the carbonyl and nitrate groups, while the slightly electron-rich, yellow-colored regions are found over the terminal phenyl and N9 atom of the purine moiety. The purine substituted methyl (C13) and C8H27 of purine are blue patches that indicate an electron deficient zone.

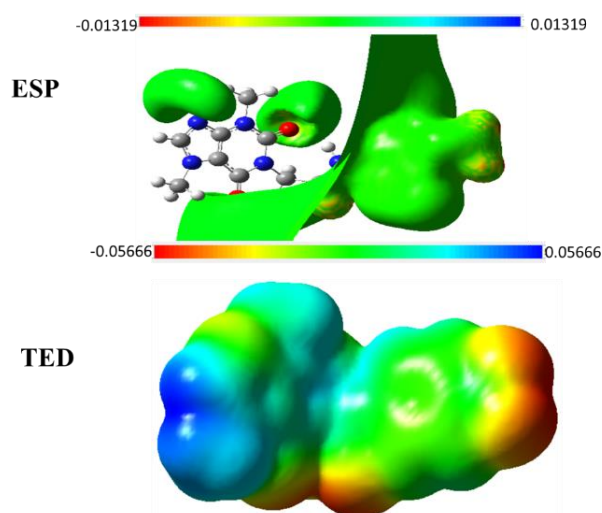


Figure 14. TED and ESP maps of T-2-PNPA at the 6-311G++(d,p) basis set.

2.6. ADMET Profiling Study

A compound becomes a drug based on its pharmacokinetic assessment and biological activity, so to prevent the late withdrawal of a new compound it should be studied early in the discovery process for ADMET properties [48]. Though ADMET identifies absorption, distribution, metabolism, excretion, and toxicity, there are a number of *in vitro* and *in vivo* studies that can explore the ADMET descriptors, but *in silico* studies are much more advantageous due to limitations of time, effort, cost, and to avoid the firm regulations governing animal testing [49]. Using Discovery studio[®], these ADMET parameters were predicted computationally for T-2-PNPA based on its reference molecule, erlotinib. The ADMET results of T-2-PNPA comparing erlotinib (Figure 15) showed an acceptable degree of drug-likeness as it was predicted to have the very low ability to pass the BBB and is expected to be non-hepatotoxic and non-inhibitor against the cytochrome P-450, CYP2D6. Additionally, as shown in Table 3, T-2-PNPA exhibited good aqueous solubility and medium intestinal absorption levels.

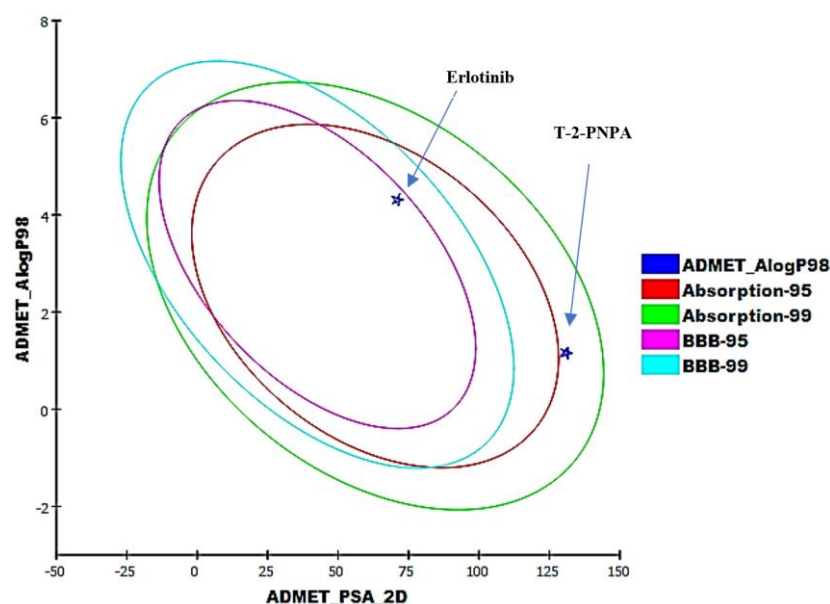


Figure 15. Computational prediction of ADMET parameters for T-2-PNPA and erlotinib.

Table 3. ADMET parameters for T-2-PNPA and erlotinib.

Comp.	BBB Level	Solubility Level	Absorption Level	Hepatotoxic Prediction	CYP2D6 Prediction	Plasma Protein Binding
T-2-PNPA	Very low	Good	Medium	Nontoxic	Noninhibitor	<90%
Erlotinib	High	Low	Good	Toxic	Noninhibitor	90%

2.7. In Silico Toxicity Studies

For the development of drugs, the early estimation of toxicity is crucial to minimize failures in later development and clinical stages [50]. The use of *in silico* methods in toxicity prediction played a crucial role in reducing time wasting and ethical issues in the traditional *in vitro* and *in vivo* testing [51]. As the important principle of *in silico* prediction of toxicity is the structure–activity relationship (SAR)-predictive toxicity, the software compares the chemical structural characteristics of the molecule with those of thousands of molecules, which have reported safety or toxicity [52]. Computing eight parameters of toxicity using Discovery studio (Table 4) indicated the general safety of T-2-PNPA comparing erlotinib.

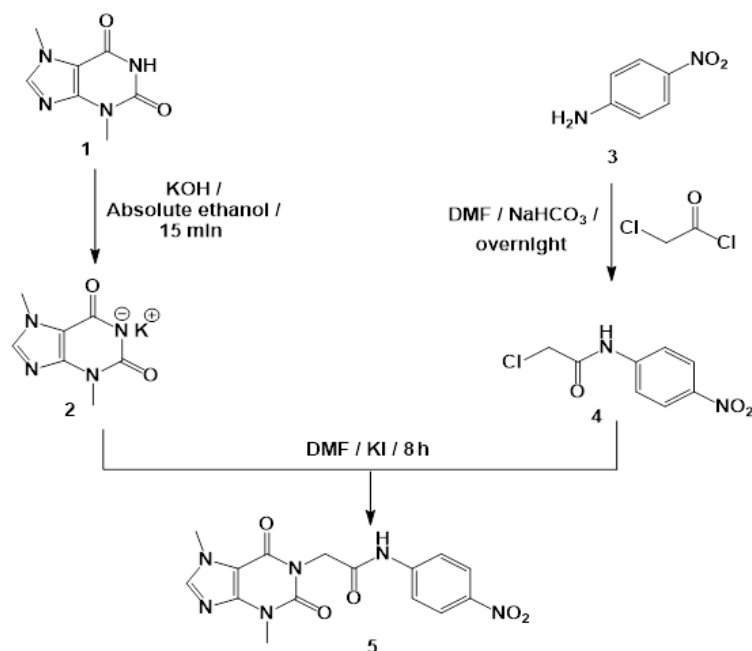
Table 4. In silico toxicity studies of T-2-PNPA and erlotinib.

Comp.	FDA Rodent Carcinogenicity (Mouse—Female)	Carcinogenic Potency TD ₅₀ (Mouse) *	Ames Mutagenicity	Rat Maximum Tolerated Dose (Feed) **	Rat Oral LD ₅₀ **	Rat Chronic LOAEL **	Skin Irritancy	Ocular Irritancy
T-2-PNPA		36.246		0.017	1.730	0.018	Mild	
Erlotinib	Non-Carcinogen	39.771	Non-Mutagen	0.083	0.662	0.036	Non-Irritant	Mild

* Unit: mg/kg /day; ** Unit: g/kg.

2.8. Chemistry

Scheme 1 described the synthetic pathway of T-2-PNPA. Initially, theobromine 1 was treated with alcoholic KOH while being continuously stirred to produce potassium salt 2 [53]. On the other hand, the 4-nitroaniline was treated with chloroacetylchloride in DMF to afford the target intermediate 4, 2-chloro-*N*-(4-nitrophenyl)acetamide. In order to finalize T-2-PNPA, the formed potassium salt 2 was then combined with 2-chloro-*N*-(4-nitrophenyl)acetamide 4 in DMF using a catalytic amount of KI.

**Scheme 1.** Synthetic pathway of T-2-PNPA.

T-2-PNPA's IR spectrum was emphasized by the appearance of absorption bands at 1709 and 1661 cm^{-1} corresponding to carbonyl groups. In addition, the ^1H NMR detected an amidic proton at 11.16 ppm. Additionally, a distinctive singlet signal for the CH_2 group could be seen at 4.76 ppm. The validity was further supported by the ^{13}C NMR spectrum, which showed distinct peaks at around 43.4, 42.5, 33.7, and 29.9 ppm for the two CH_2 and two CH_3 moieties, respectively.

2.9. Biological Evaluation

2.9.1. In Vitro EGFR Inhibition

To verify the conducted computational results, the potentialities of T-2-PNPA against both wild subtype, EGFR^{WT}, and the mutant subtype EGFR^{T790M} of EGFR protein were investigated in vitro. T-2-PNPA firmly inhibited both proteins with IC₅₀ values of 7.05 and 126.20 nM, respectively. Those results (Figure 16) were bordering erlotinib's value (5.91 nM) against EGFR^{WT} and much stronger than that against EGFR^{T790M} (202.40 nM).

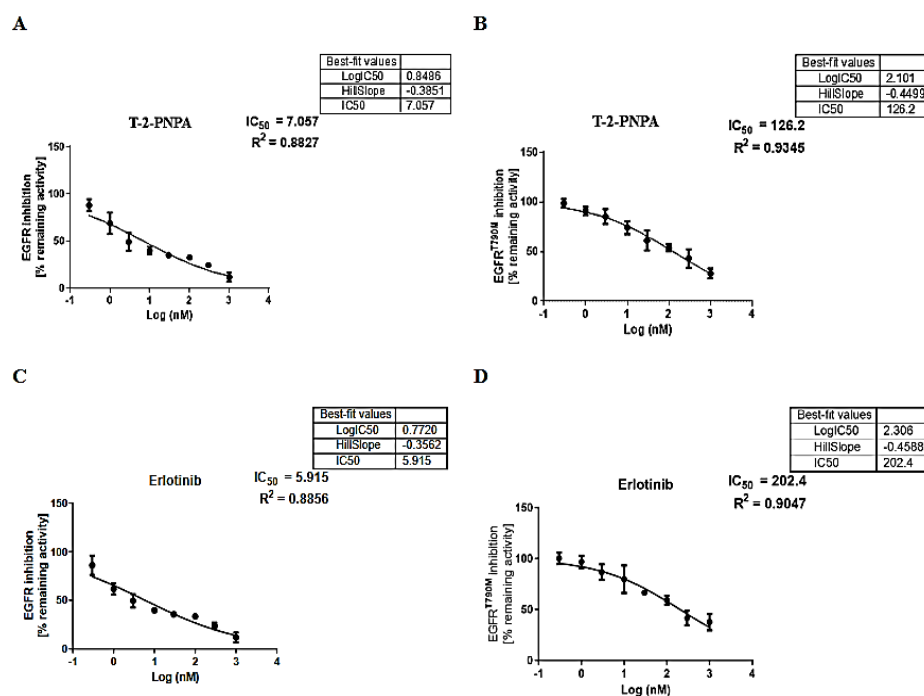


Figure 16. In vitro inhibition of T-2-PNPA against EGFR^{WT} (A) and EGFR^{T790M} (B) compared with erlotinib's activities against EGFR^{WT} (C) and EGFR^{T790M} (D).

The preceded computational studies (design, molecular docking, MD simulations, MM-GPSA, and DFT calculations) predicted the potentialities of T-2-PNPA to bind correctly and inhibit both types of EGFR protein (EGFR^{WT} and EGFR^{T790M}). These in silico results were highly in consonance with the obtained results of the in vitro assay of T-2-PNPA against EGFR^{WT} and EGFR^{T790M}.

2.9.2. Cytotoxicity

Because T-2-PNPA showed good inhibitory (in silico and in vitro) potentialities against EGFR^{WT} and EGFR^{T790M}, it is predicted to express promising anticancer effects. Accordingly, the cytotoxicity of T-2-PNPA was assessed in vitro against A549 and HCT-116 malignant besides WI-38 normal cell lines using erlotinib as a reference drug. Table 5 shows that T-2-PNPA expressed anticancer properties almost the same as erlotinib, but with much higher safety. In detail, T-2-PNPA inhibited the growth of the malignant cells with IC₅₀ values of 11.09 and 21.01 μ M, respectively. Additionally, it was determined that T-2-PNPA demonstrated an excellent level of safety against WI-38 cell lines (Figure 17), exhibiting a high IC₅₀ value of 48.06 μ M and very high selectivity indices (SI) against cancer cell lines of 4.3 and 2.3, respectively.

Table 5. In vitro anti-proliferative and safety assessment of T-2-PNPA against A549, HCT-116 and WI-38 cell lines.

Comp.	In Vitro Cytotoxicity IC ₅₀ (μ M) ^a			A549 (SI)	HCT-116 (SI)	EGFR ^{WT} IC ₅₀ (nM)	EGFR ^{T790M} IC ₅₀ (nM)
	A549	HCT-116	WI-38				
T-2-PNPA	11.09	21.01	48.06	4.3	2.3	7.05	126.20
Erlotinib	6.73	16.35	31.17	4.6	1.9	5.91	202.40

^a Data are expressed as three times' IC₅₀ values mean.

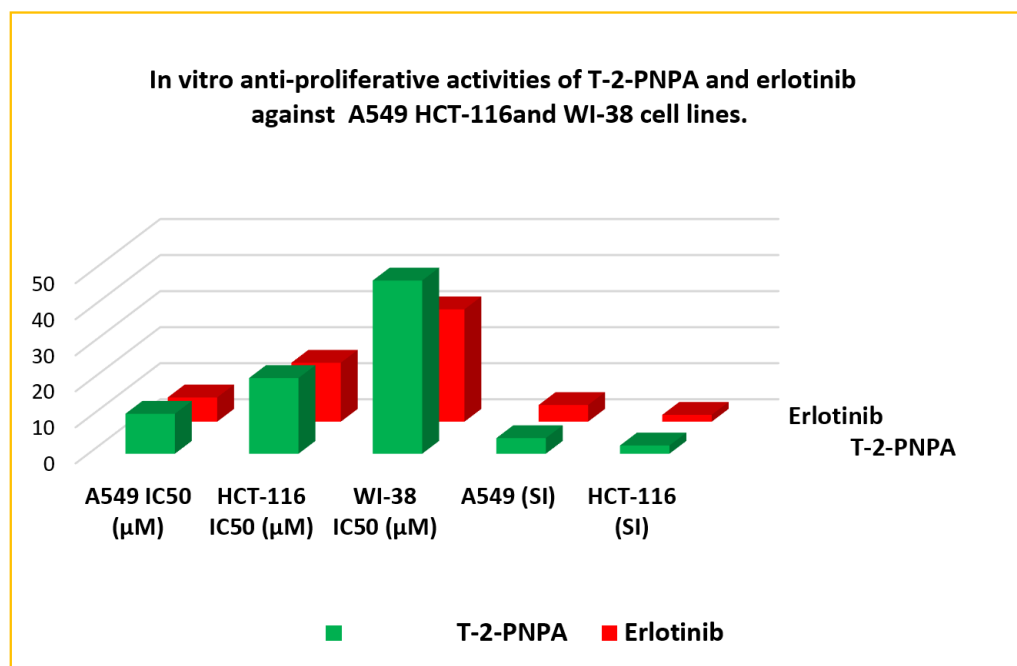


Figure 17. In vitro anti-proliferative and safety assessment of T-2-PNPA against A549, HCT-116, and WI-38 cell lines.

3. Experimental Section

3.1. In Silico Studies

3.1.1. Docking Studies

The molecular docking of T-2-PNPA was accomplished by MOE2014 software [54]. Supplementary Materials show a comprehensive explanation.

3.1.2. MD Simulations

MD simulations were accomplished by CHARMM-GUI web server (V 3.8) and GRO-MACS 2021 as MD engines [55]. Supplementary Materials show a comprehensive explanation.

3.1.3. MM-GBSA

MM-GBSA was accomplished by the Gmx_MMPBSA (V 1.5.6) package. Supplementary Materials show a comprehensive explanation.

3.1.4. DFT

DFT was accomplished by Gaussian 09 and GaussSum3.0 programs. Supplementary Materials show a comprehensive explanation.

3.1.5. ADMET Studies

The ADMET profile of T-2-PNPA was accomplished by Discovery Studio 4.0 [56]. Supplementary Materials show a comprehensive explanation.

3.1.6. Toxicity Studies

The toxicity profile of T-2-PNPA was accomplished by Discovery Studio 3.0 [57]. Supplementary Materials show a comprehensive explanation.

3.2. Synthesis of T-2-PNPA

Supplementary Materials show a comprehensive explanation.

3.3. Biological Studies

3.3.1. In Vitro EGFR Inhibition

This was accomplished by Human EGFR ELISA kit, Thermo Fisher Scientific, USA. Supplementary Materials show a comprehensive explanation.

3.3.2. In Vitro Antiproliferative Activity

MTT procedure was performed [58,59]. Supplementary Materials show a comprehensive explanation.

3.3.3. Safety Assay

The normal cell lines, W138, were utilized. Supplementary Materials show a comprehensive explanation.

4. Conclusions

T-2-PNPA is a 2-N-(4-nitrophenyl)acetamide derivative of theobromine that was designed to inhibit the EGFR protein according to its essential structural properties. Based on molecular docking, **T-2-PNPA** showed a high potential anti-EGFR^{WT} and EGFR^{T790M} activities, which was verified through six MD (over 100 ns) and three MM-GBSA, as well as three DFT studies. In addition, ADMET analysis examined the safety and likeness of **T-2-PNPA**. Consequently, **T-2-PNPA** was prepared and it inhibited EGFR^{WT} and EGFR^{T790M} with IC₅₀ values of 7.05 and 126.20 nM, respectively. **T-2-PNPA** also inhibited A549 and HCT-116 cells with IC₅₀ values of 11.09 and 21.01 μM, respectively, exhibiting selectivity indices of 4.3 and 2.3. We introduce **T-2-PNPA** for the first time as a promising anticancer lead compound for further biological studies as well as chemical modifications.

Supplementary Materials: The following supporting information can be downloaded at: <https://www.mdpi.com/article/10.3390/pr10112290/s1>

Author Contributions: Project administration, A.M.M., I.H.E.; Supervision, I.H.E.; Funding acquisition, E.B.E., A.A.A.; Methodology, R.G.Y., M.A., H.E., D.Z.H. and I.M.I., H.S.A.E.; Validation, I.H.E.; Writing—original draft, H.E.; Writing—review and editing, E.B.E., A.A.A., A.M.M. and I.H.E. All authors have read and agreed to the published version of the manuscript.

Funding: This research was funded by Princess Nourah bint Abdulrahman University Researchers Supporting Project number (PNURSP2022R116), Princess Nourah bint Abdulrahman University, Riyadh, Saudi Arabia. The authors extend their appreciation to the Research Center at AlMaarefa University for funding this work.

Data Availability Statement: Data are available with corresponding authors upon request.

Conflicts of Interest: No conflict of interest to be declared.

References

1. WHO Cancer, Fact Sheet. Available online: <https://www.who.int/news-room/fact-sheets/detail/cancer> (accessed on 13 June 2022).
2. Chaudhari, P.; Bari, S.; Surana, S.; Shirkhedkar, A.; Wakode, S.; Shelar, S.; Racharla, S.; Ugale, V.; Ghodke, M. Logical synthetic strategies and structure-activity relationship of indolin-2-one hybrids as small molecule anticancer agents: An Overview. *J. Mol. Struct.* **2021**, *1247*, 131280. [[CrossRef](#)]
3. Lugano, R.; Ramachandran, M.; Dimberg, A. Tumor angiogenesis: Causes, consequences, challenges and opportunities. *Cell. Mol. Life Sci.* **2020**, *77*, 1745–1770. [[CrossRef](#)] [[PubMed](#)]
4. El-Dash, Y.; Elzayat, E.; Abdou, A.M.; Hassan, R.A. Novel thienopyrimidine-aminothiazole hybrids: Design, synthesis, antimicrobial screening, anticancer activity, effects on cell cycle profile, caspase-3 mediated apoptosis and VEGFR-2 inhibition. *Bioorganic Chem.* **2021**, *114*, 105137. [[CrossRef](#)] [[PubMed](#)]
5. Nicholson, R.I.; Gee, J.M.W.; Harper, M.E. EGFR and cancer prognosis. *Eur. J. Cancer* **2001**, *37*, 9–15. [[CrossRef](#)]
6. Hashmi, A.A.; Naz, S.; Hashmi, S.K.; Irfan, M.; Hussain, Z.F.; Khan, E.Y.; Asif, H.; Faridi, N. Epidermal growth factor receptor (EGFR) overexpression in triple-negative breast cancer: Association with clinicopathologic features and prognostic parameters. *Surg. Exp. Pathol.* **2019**, *2*, 6. [[CrossRef](#)]

7. Spano, J.-P.; Lagorce, C.; Atlan, D.; Milano, G.; Domont, J.; Benamouzig, R.; Attar, A.; Benichou, J.; Martin, A.; Morere, J.-F. Impact of EGFR expression on colorectal cancer patient prognosis and survival. *Ann. Oncol.* **2005**, *16*, 102–108. [[CrossRef](#)]
8. Normanno, N.; De Luca, A.; Bianco, C.; Strizzi, L.; Mancino, M.; Maiello, M.R.; Carotenuto, A.; De Feo, G.; Caponigro, F.; Salomon, D.S. Epidermal growth factor receptor (EGFR) signaling in cancer. *Gene* **2006**, *366*, 2–16. [[CrossRef](#)]
9. Ayati, A.; Moghimi, S.; Salarinejad, S.; Safavi, M.; Pouramiri, B.; Foroumadi, A. A review on progression of epidermal growth factor receptor (EGFR) inhibitors as an efficient approach in cancer targeted therapy. *Bioorg. Chem.* **2020**, *99*, 103811. [[CrossRef](#)]
10. Metwaly, A.M.; Ghoneim, M.M.; Eissa, I.H.; Elsehemy, I.A.; Mostafa, A.E.; Hegazy, M.M.; Afifi, W.M.; Dou, D. Traditional ancient Egyptian medicine: A review. *Saudi J. Biol. Sci.* **2021**, *28*, 5823–5832. [[CrossRef](#)]
11. Han, X.; Yang, Y.; Metwaly, A.M.; Xue, Y.; Shi, Y.; Dou, D. The Chinese herbal formulae (Yitangkang) exerts an antidiabetic effect through the regulation of substance metabolism and energy metabolism in type 2 diabetic rats. *J. Ethnopharmacol.* **2019**, *239*, 111942. [[CrossRef](#)]
12. Newman, D.J.; Cragg, G.M. Natural products as sources of new drugs from 1981 to 2014. *J. Nat. Prod.* **2016**, *79*, 629–661. [[CrossRef](#)] [[PubMed](#)]
13. Barcz, E.; Sommer, E.; Janik, P.; Marianowski, L.; Skopinska-Rozewska, E. Adenosine receptor antagonism causes inhibition of angiogenic activity of human ovarian cancer cells. *Oncol. Rep.* **2000**, *7*, 1285–1376. [[CrossRef](#)] [[PubMed](#)]
14. Kakuyamanee Iwazaki, A.; Sadzuka, Y. Effect of methylxanthine derivatives on doxorubicin transport and antitumor activity. *Curr. Drug Metab.* **2001**, *2*, 379–395. [[CrossRef](#)] [[PubMed](#)]
15. Sultani, H.N.; Ghazal, R.A.; Hayallah, A.M.; Abdulrahman, L.K.; Abu-Hammour, K.; AbuHammad, S.; Taha, M.O.; Zihlif, M.A. Inhibitory effects of new mercapto xanthine derivatives in human mcf7 and k562 cancer cell lines. *J. Heterocycl. Chem.* **2017**, *54*, 450–456. [[CrossRef](#)]
16. Woskresensky, A. Ueber das Theobromin. *Justus Liebigs Ann. Der Chem.* **1842**, *41*, 125–127. [[CrossRef](#)]
17. Smit, H.J. Theobromine and the pharmacology of cocoa. *Methylxanthines* **2011**, 201–234.
18. Sugimoto, N.; Miwa, S.; Hitomi, Y.; Nakamura, H.; Tsuchiya, H.; Yachie, A. Theobromine, the primary methylxanthine found in Theobroma cacao, prevents malignant glioblastoma proliferation by negatively regulating phosphodiesterase-4, extracellular signal-regulated kinase, Akt/mammalian target of rapamycin kinase, and nuclear factor-kappa B. *Nutr. Cancer* **2014**, *66*, 419–423.
19. Gil, M.; Skopińska-Rózewska, E.; Radomska, D.; Demkow, U.; Skurzak, H.; Rochowska, M.; Beuth, J.; Roszkowski, K. Effect of purinergic receptor antagonists suramin and theobromine on tumor-induced angiogenesis in BALB/c mice. *Folia Biol.* **1993**, *39*, 63–68.
20. Barcz, E.; Sommer, E.; Sokolnicka, I.; Gawrychowski, K.; Roszkowska-Purska, K.; Janik, P.; Skopinska-Rózewska, E. The influence of theobromine on angiogenic activity and proangiogenic cytokines production of human ovarian cancer cells. *Oncol. Rep.* **1998**, *5*, 517–537. [[CrossRef](#)]
21. da Rosa, R.; Schenkel, E.P.; Bernardes, L.S.C. Semisynthetic and newly designed derivatives based on natural chemical scaffolds: Moving beyond natural products to fight Trypanosoma cruzi. *Phytochem. Rev.* **2020**, *19*, 105–122. [[CrossRef](#)]
22. Mahmoud, A.H.; Masters, M.R.; Yang, Y.; Lill, M.A. Elucidating the multiple roles of hydration for accurate protein-ligand binding prediction via deep learning. *Commun. Chem.* **2020**, *3*, 19. [[CrossRef](#)]
23. Elton, D.C.; Boukouvalas, Z.; Fuge, M.D.; Chung, P.W. Engineering, Deep learning for molecular design—A review of the state of the art. *Mol. Syst. Des. Eng.* **2019**, *4*, 828–849. [[CrossRef](#)]
24. Keith, J.A.; Vassilev-Galindo, V.; Cheng, B.; Chmiela, S.; Gastegger, M.; Müller, K.R.; Tkatchenko, A. Combining machine learning and computational chemistry for predictive insights into chemical systems. *Chem. Rev.* **2021**, *121*, 9816–9872. [[CrossRef](#)]
25. Cáceres, E.L.; Tudor, M.; Cheng, A.C. Deep learning approaches in predicting ADMET properties. *Future Med. Chem.* **2020**, *12*, 1995–1999. [[CrossRef](#)] [[PubMed](#)]
26. Ciallella, H.L.; Zhu, H. Advancing computational toxicology in the big data era by artificial intelligence: Data-driven and mechanism-driven modeling for chemical toxicity. *Chem. Res. Toxicol.* **2019**, *32*, 536–547. [[CrossRef](#)] [[PubMed](#)]
27. Tielens, F.; Gierada, M.; Handzlik, J.; Calatayud, M. Characterization of amorphous silica based catalysts using DFT computational methods. *Catal. Today* **2020**, *354*, 3–18. [[CrossRef](#)]
28. Pracht, P.; Bohle, F.; Grimme, S. Automated exploration of the low-energy chemical space with fast quantum chemical methods. *Phys. Chem. Chem. Phys.* **2020**, *22*, 7169–7192. [[CrossRef](#)]
29. Seidel, T.; Schuetz, D.A.; Garon, A.; Langer, T. The pharmacophore concept and its applications in computer-aided drug design. *Prog. Chem. Org. Nat. Prod.* **2019**, *110*, 99–141.
30. Bonomi, P. Erlotinib: A new therapeutic approach for non-small cell lung cancer. *Expert Opin. Investig. Drugs* **2003**, *12*, 1395–1401. [[CrossRef](#)]
31. Ou, S.-H.I. Second-generation irreversible epidermal growth factor receptor (EGFR) tyrosine kinase inhibitors (TKIs): A better mousetrap? A review of the clinical evidence. *Crit. Rev. Oncol. Hematol.* **2012**, *83*, 407–421. [[CrossRef](#)]
32. Jänne, P.A.; Yang, J.C.-H.; Kim, D.-W.; Planchard, D.; Ohe, Y.; Ramalingam, S.S.; Ahn, M.-J.; Kim, S.-W.; Su, W.-C.; Horn, L. AZD9291 in EGFR inhibitor-resistant non-small-cell lung cancer. *N. Engl. J. Med.* **2015**, *372*, 1689–1699. [[CrossRef](#)] [[PubMed](#)]
33. Xu, X. Parallel phase 1 clinical trials in the US and in China: Accelerating the test of avitinib in lung cancer as a novel inhibitor selectively targeting mutated EGFR and overcoming T790M—Induced resistance. *Cancer Commun.* **2015**, *34*, 1–3. [[CrossRef](#)] [[PubMed](#)]

34. Traxler, P.; Bold, G.; Frei, J.; Lang, M.; Lydon, N.; Mett, H.; Buchdunger, E.; Meyer, T.; Mueller, M.; Furet, P. Use of a pharmacophore model for the design of EGF-R tyrosine kinase inhibitors: 4-(phenylamino) pyrazolo [3, 4-d] pyrimidines. *J. Med. Chem.* **1997**, *40*, 3601–3616. [[CrossRef](#)] [[PubMed](#)]
35. Ducray, R.; Ballard, P.; Barlaam, B.C.; Hickinson, M.D.; Kettle, J.G.; Ogilvie, D.J.; Trigwell, C.B. Novel 3-alkoxy-1H-pyrazolo [3, 4-d] pyrimidines as EGFR and erbB2 receptor tyrosine kinase inhibitors. *Bioorg. Med. Chem. Lett.* **2008**, *18*, 959–962. [[CrossRef](#)]
36. Gaber, A.A.; Bayoumi, A.H.; El-Morsy, A.M.; Sherbiny, F.F.; Mehany, A.B.; Eissa, I.H. Design, synthesis and anticancer evaluation of 1H-pyrazolo [3, 4-d] pyrimidine derivatives as potent EGFRWT and EGFR790M inhibitors and apoptosis inducers. *Bioorg. Chem.* **2018**, *80*, 375–395. [[CrossRef](#)]
37. Elmetwally, S.A.; Saied, K.F.; Eissa, I.H.; Elkaeed, E.B. Design, synthesis and anticancer evaluation of thieno [2, 3-d] pyrimidine derivatives as dual EGFR/HER2 inhibitors and apoptosis inducers. *Bioorg. Chem.* **2019**, *88*, 102944. [[CrossRef](#)]
38. Elzahabi, H.S.; Nossier, E.S.; Alasfoury, R.A.; El-Manawaty, M.; Sayed, S.M.; Elkaeed, E.B.; Metwaly, A.M.; Hagra, M.; Eissa, I.H. Design, synthesis, and anti-cancer evaluation of new pyrido [2, 3-d] pyrimidin-4 (3H)-one derivatives as potential EGFRWT and EGFR790M inhibitors and apoptosis inducers. *J. Enzym. Inhib. Med. Chem.* **2022**, *37*, 1053–1076. [[CrossRef](#)]
39. Gandin, V.; Ferrarese, A.; Dalla Via, M.; Marzano, C.; Chilin, A.; Marzaro, G. Targeting kinases with anilinopyrimidines: Discovery of N-phenyl-N'-[4-(pyrimidin-4-ylamino) phenyl] urea derivatives as selective inhibitors of class III receptor tyrosine kinase subfamily. *Sci. Rep.* **2015**, *5*, 16750. [[CrossRef](#)]
40. Liu, Y.; Gray, N.S. Rational design of inhibitors that bind to inactive kinase conformations. *Nat. Chem. Biol.* **2006**, *2*, 358–364. [[CrossRef](#)]
41. Furet, P.; Caravatti, G.; Lydon, N.; Priestle, J.P.; Sowadski, J.M.; Trinks, U.; Traxler, P. Modelling study of protein kinase inhibitors: Binding mode of staurosporine and origin of the selectivity of CGP 52411. *J. Comput. Aided Mol. Des.* **1995**, *9*, 465–472. [[CrossRef](#)]
42. Eldehna, W.M.; El Hassab, M.A.; Elsayed, Z.M.; Al-Warhi, T.; Elkady, H.; Abo-Ashour, M.F.; Abourehab, M.A.; Eissa, I.H.; Abdel-Aziz, H.A. Design, synthesis, in vitro biological assessment and molecular modeling insights for novel 3-(naphthalen-1-yl)-4, 5-dihydropyrazoles as anticancer agents with potential EGFR inhibitory activity. *Sci. Rep.* **2022**, *12*, 12821. [[CrossRef](#)] [[PubMed](#)]
43. Gonçalves, M.A.; Santos, L.S.; Prata, D.M.; Peixoto, F.C.; da Cunha, E.F.; Ramalho, T.C. Optimal wavelet signal compression as an efficient alternative to investigate molecular dynamics simulations: Application to thermal and solvent effects of MRI probes. *Theor. Chem. Acc.* **2017**, *136*, 15. [[CrossRef](#)]
44. Husein, D.Z.; Hassanien, R.; Khamis, M. Cadmium oxide nanoparticles/graphene composite: Synthesis, theoretical insights into reactivity and adsorption study. *RSC Adv.* **2021**, *11*, 27027–27041. [[CrossRef](#)] [[PubMed](#)]
45. Wang, T.; Husein, D.Z. Novel synthesis of multicomponent porous nano-hybrid composite, theoretical investigation using DFT and dye adsorption applications: Disposing of waste with waste. *Environ. Sci. Pollut. Res.* **2022**, 1–28. [[CrossRef](#)] [[PubMed](#)]
46. La Porta, F.A.; Ramalho, T.C.; Santiago, R.T.; Rocha, M.V.; da Cunha, E.F. Orbital signatures as a descriptor of regioselectivity and chemical reactivity: The role of the frontier orbitals on 1, 3-dipolar cycloadditions. *J. Phys. Chem. A* **2011**, *115*, 824–833. [[CrossRef](#)]
47. Coelho, J.V.; Freitas, M.P.; Ramalho, T.C.; Martins, C.R.; Bitencourt, M.; Cormanich, R.A.; Tormena, C.F.; Rittner, R. The case of infrared carbonyl stretching intensities of 2-bromocyclohexanone: Conformational and intermolecular interaction insights. *Chem. Phys. Lett.* **2010**, *494*, 26–30. [[CrossRef](#)]
48. Ferreira, L.L.; Andricopulo, A.D. ADMET modeling approaches in drug discovery. *Drug Discov. Today* **2019**, *24*, 1157–1165. [[CrossRef](#)]
49. Norinder, U.; Bergström, C.A. Prediction of ADMET properties. *ChemMedChem Chem. Enabling Drug Discov.* **2006**, *1*, 920–937.
50. Dearden, J.C. In silico prediction of drug toxicity. *J. Comput.-Aided Mol. Des.* **2003**, *17*, 119–127. [[CrossRef](#)]
51. Idakwo, G.; Luttrell, J.; Chen, M.; Hong, H.; Zhou, Z.; Gong, P.; Zhang, C. A review on machine learning methods for in silico toxicity prediction. *J. Environ. Sci. Health Part C* **2018**, *36*, 169–191. [[CrossRef](#)]
52. Kruhlak, N.; Benz, R.; Zhou, H.; Colatsky, T. (Q) SAR modeling and safety assessment in regulatory review. *Clin. Pharmacol. Ther.* **2012**, *91*, 529–534. [[CrossRef](#)] [[PubMed](#)]
53. Elkaeed, E.B.; Yousef, R.G.; Elkady, H.; Alsouk, A.A.; Husein, D.Z.; Ibrahim, I.M.; Metwaly, A.M.; Eissa, I.H. New Anticancer Theobromine Derivative Targeting EGFRWT and EGFR790M: Design, Semi-Synthesis, In Silico, and In Vitro Anticancer Studies. *Molecules* **2022**, *27*, 5859. [[CrossRef](#)] [[PubMed](#)]
54. Eissa, I.H.; Alesawy, M.S.; Saleh, A.M.; Elkaeed, E.B.; Alsouk, B.A.; El-Attar, A.-A.M.; Metwaly, A.M. Ligand and structure-based in silico determination of the most promising SARS-CoV-2 nsp16-nsp10 2'-O-Methyltransferase complex inhibitors among 3009 FDA approved drugs. *Molecules* **2022**, *27*, 2287. [[CrossRef](#)] [[PubMed](#)]
55. Suleimen, Y.M.; Jose, R.A.; Suleimen, R.N.; Arenz, C.; Ishmuratova, M.; Toppet, S.; Dehaen, W.; Alsouk, A.A.; Elkaeed, E.B.; Eissa, I.H. Isolation and In Silico Anti-SARS-CoV-2 Papain-Like Protease Potentialities of Two Rare 2-Phenoxychromone Derivatives from *Artemisia* spp. *Molecules* **2022**, *27*, 1216. [[CrossRef](#)]
56. Suleimen, Y.M.; Jose, R.A.; Suleimen, R.N.; Arenz, C.; Ishmuratova, M.Y.; Toppet, S.; Dehaen, W.; Alsouk, B.A.; Elkaeed, E.B.; Eissa, I.H. Jusanin, a New Flavonoid from *Artemisia commutata* with an In Silico Inhibitory Potential against the SARS-CoV-2 Main Protease. *Molecules* **2022**, *27*, 1636. [[CrossRef](#)]
57. Mohammed, S.O.; El Ashry, E.S.H.; Khalid, A.; Amer, M.R.; Metwaly, A.M.; Eissa, I.H.; Elkaeed, E.B.; Elshobaky, A.; Hafez, E.E. Expression, Purification, and Comparative Inhibition of *Helicobacter pylori* Urease by Regio-Selectively Alkylated Benzimidazole 2-Thione Derivatives. *Molecules* **2022**, *27*, 865. [[CrossRef](#)]

-
58. Alanazi, M.M.; Elkady, H.; Alsaif, N.A.; Obaidullah, A.J.; Alkahtani, H.M.; Alanazi, M.M.; Alharbi, M.A.; Eissa, I.H.; Dahab, M.A. New quinoxaline-based VEGFR-2 inhibitors: Design, synthesis, and antiproliferative evaluation with in silico docking, ADMET, toxicity, and DFT studies. *RSC Adv.* **2021**, *11*, 30315–30328. [[CrossRef](#)]
 59. Alanazi, M.M.; Elkady, H.; Alsaif, N.A.; Obaidullah, A.J.; Alanazi, W.A.; Al-Hossaini, A.M.; Alharbi, M.A.; Eissa, I.H.; Dahab, M.A. Discovery of new quinoxaline-based derivatives as anticancer agents and potent VEGFR-2 inhibitors: Design, synthesis, and in silico study. *J. Mol. Struct.* **2021**, *1253*, 132220. [[CrossRef](#)]